Thermal tuning of infrared resonant absorbers based on hybrid gold-VO$_2$ nanostructures

Hasan Kocer, Serkan Butun, Berker Banar, Kevin Wang, Sefaatttin Tongay, Junqiao Wu, and Koray Aydin

Thermal tuning of infrared resonant absorbers based on hybrid gold-VO$_2$ nanostructures

Hasan Kocer,[1,2,a)] Serkan Butun,[1,a)] Berker Banar,[1,3] Kevin Wang,[4] Sefaatttin Tongay,[5] Junqiao Wu,[4] and Koray Aydin[1,b)]

[1]*Department of Electrical Engineering and Computer Science, Northwestern University, Evanston, Illinois 60208, USA*
[2]*Department of Electrical Engineering, Turkish Military Academy, 06654 Ankara, Turkey*
[3]*Department of Electrical and Electronics Engineering, Bilkent University, 06800 Bilkent, Ankara, Turkey*
[4]*Department of Materials Science and Engineering, University of California Berkeley, Berkeley, California 94720, USA*
[5]*School for Engineering of Matter, Transport and Energy, Arizona State University, Tempe, Arizona 85287, USA*

Resonant absorbers based on plasmonic materials, metamaterials, and thin films enable spectrally selective absorption filters, where absorption is maximized at the resonance wavelength. By controlling the geometrical parameters of nano/microstructures and materials' refractive indices, resonant absorbers are designed to operate at wide range of wavelengths for applications including absorption filters, thermal emitters, thermophotovoltaic devices, and sensors. However, once resonant absorbers are fabricated, it is rather challenging to control and tune the spectral absorption response. Here, we propose and demonstrate thermally tunable infrared resonant absorbers using hybrid gold-vanadium dioxide (VO$_2$) nanostructure arrays. Absorption intensity is tuned from 90% to 20% and 96% to 32% using hybrid gold-VO$_2$ nanowire and nanodisc arrays, respectively, by heating up the absorbers above the phase transition temperature of VO$_2$ (68 °C). Phase change materials such as VO$_2$ deliver useful means of altering optical properties as a function of temperature. Absorbers with tunable spectral response can find applications in sensor and detector applications, in which external stimulus such as heat, electrical signal, or light results in a change in the absorption spectrum and intensity. © *2015 AIP Publishing LLC*.
[http://dx.doi.org/10.1063/1.4918938]

Electromagnetic absorbers based on structured surfaces including metamaterial and plasmonic nanostructures have received burgeoning amount of attention in recent years and have enabled spectrally selective absorption over microwave,[1] terahertz,[1] infrared (IR),[2–6] and visible[7–9] bands of electromagnetic spectrum. In particular, controlling and manipulating the spectral absorption properties of materials in the IR range are an active area of research and could enable advances in applications such as target recognition, biochemical sensing, camouflage, IR signature mimicry, imaging, sensors, IR labelling, and wavelength selective IR sources.[10,11] Having a tunable resonance response for IR wavelength range is a desired feature for thermal emitters,[12] thermophotovoltaic cells,[2] as well as plasmonic scatters.[13–15]

In this study, we propose and demonstrate intensity-tunable short-wavelength infrared nanostructured resonant absorbers by utilizing a phase change material, vanadium dioxide (VO$_2$). VO$_2$ undergoes a structural transition from an insulating phase to a metallic phase at the transition temperature of 68 °C. This reversible phase change occurs on a sub-picosecond timescale.[16,17] Around the phase transition temperature, metallic VO$_2$ (m-VO$_2$) islands occurs inside the insulating VO$_2$ (i-VO$_2$) and as the temperature increases, the entire VO$_2$ film becomes metallic. The phase transition of VO$_2$ is mediated by heating the absorber device over the transition temperature.

We theoretically and experimentally investigated two different absorbers, (i) Au - VO$_2$ periodic gratings and (ii) Au cylinders embedded in VO$_2$. Our two hybrid gold-VO$_2$ nanostructured absorber designs are schematically depicted in Figs. 1(a) and 1(b). While the former exploits discrete VO$_2$ stripes embedded in a gold matrix, the latter utilizes a 2D square lattice of gold cylinders embedded in VO$_2$. We will refer to these two different designs as "g-design" (Fig. 1(a)) and "c-design" (Fig. 1(b)) throughout this paper. Each structure has an optically thick Au layer (100 nm) as a backside reflector to ensure that there is no light transmission. In addition, samples are illuminated from the sapphire side.

Our proposed tunable absorbers are fabricated on epitaxially grown VO$_2$ layers on double side polished sapphire substrate using conventional e-beam lithography and deposition techniques. The details of the fabrication methods can be found in supplementary material.[18] The scanning electron microscope (SEM) images of fabricated g-design and c-design structures are shown in Figs. 1(c) and 1(d), respectively. Note that the deposition of Au layer was conducted after patterning the VO$_2$ layer. Therefore, SEM images in Figs. 1(c) and 1(d) depict the topography of the gold surface which follows the underlying VO$_2$ pattern. This is clearly visible in the cross-sectional focused ion beam (FIB) image

[a)]H. Kocer and S. Butun contributed equally to this work.
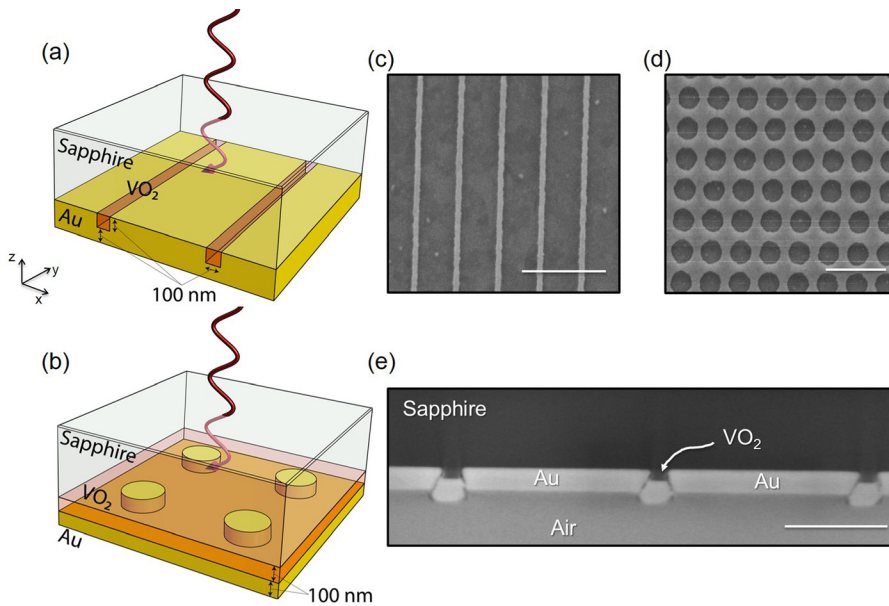[b)]Author to whom correspondence should be addressed. Electronic mail: aydin@northwestern.edu

FIG. 1. Tunable IR absorber designs. The schematic representations of grating (a) and cylinder (b) hybrid gold-VO$_2$ design, respectively. Relevant design parameters are indicated on the figures. (c) and (d) Scanning electron microscope images of the grating and cylindrical devices illustrated in (a) and (b), respectively. Scale bars correspond to 2 μm. Both of the images are acquired subsequent to gold deposition. (e) Focused ion beam cross-sectional image of the grating design. The scale bar corresponds to 500 nm. The sample tilt is 45°.

given in Fig. 1(e). The actual width of the VO$_2$ stripes in g-design (and diameter of the cylinders in c-design) turns out to be narrower than those measured in the SEM images, which is taken in to account in our numerical calculations.

For a profound analysis of structures, we have performed full field finite difference time domain (FDTD) simulations using a commercial grade solver Lumerical FDTD.[19] The experimental refractive index data of VO$_2$ reported by Dicken *et al.*[16] were utilized in FDTD simulations. The total absorption in the hybrid gold-VO$_2$ structure is calculated by 1–*R-T*, where *R* is the total reflection at the sapphire side and *T* is the transmission which is zero due to the optically thick gold mirror at the back side. Therefore, the total absorption can be calculated as 1–*R* in both measurements and simulations. The spectral reflectivity measurements were performed by a Fourier transform IR (FTIR) spectroscopy coupled with a heating stage and IR microscope. Please refer to supplementary material[18] for detailed explanation of the methods used for measurements and simulations. Simulated and measured absorption spectra for the hybrid Au-VO$_2$ wire-gratings of periodicity, Λ, 1 μm for polarization along and parallel to stripes are shown in Fig. 2. As for any 1D grating structure, we observe an optical resonance when electric field is perpendicular to stripes. FDTD simulations revealed two distinct resonances at 1.7 and 2.6 μm (Fig. 2(a) blue curve). The first resonance at 1.7 μm is at about $n_{eff} \times \Lambda$ which is the lattice mode of the gold grating, where n_{eff} is the effective refractive index. Note that VO$_2$ stripes between the gold ridges make the effective refractive index slightly larger than refractive index of sapphire. The second mode at 2.6 μm is the localized mode within the grooves of the underlying gold grating where VO$_2$ fills. The FTIR spectroscopy measurements (Fig. 2(c) blue curve) confirm this phenomenon with a broadening of the first and a slight blue shift of the second resonance wavelengths. The broadening of the first resonance is due the high numerical aperture of the illumination objective (0.4) which effectively illuminates the sample with a broad range of in-plane momentum. We attribute the slight blue shift of the second resonance to poor fit of readily

available index data of VO$_2$ to our samples because this resonance is highly sensitive to the refractive index of VO$_2$. Whereas the dependence of the lattice resonance to the refractive index of VO$_2$ is minor. As expected, there is no resonance observed for the other polarization in neither simulations nor measurements (Figs. 2(b) and 2(d)). We additionally note that due to imperfections aroused during the fabrication, we have a further mismatch between the measured and simulated absorption spectra in terms of amplitude especially towards the long end of the spectrum.

The extraordinary behavior of the IR absorber occurs when we heat the sample above the critical phase change temperature (68 °C). At an elevated temperature above the critical point (120 °C in our measurements), VO$_2$ becomes metallic, which substantially alters the refractive index compared to the insulating phase below the critical point. The hybrid gold-VO$_2$ structure at high temperatures behaves like a continuous reflective surface. As a result, the absorption is dramatically suppressed (Figs. 2(a) and 2(c) red curves). Here, we theoretically and experimentally demonstrate an intensity tunable absorber between 2 μm and 3 μm such that absorption can be either suppressed or enhanced in a positive dynamic range depending on the phase of the VO$_2$. 9-fold and 4.5-fold increase at the resonance in the absorption intensity is obtained theoretically and experimentally, respectively, when the polarization of incident light is perpendicular to the grating.

According to Kirchhoff's law of thermal radiation, the emissivity, *E*, of a material is equal to its absorptivity, *A*, at thermal equilibrium.[20] If the absorptivity, therefore emissivity decreases as the temperature rises, the thermochromic structure has a positive dynamic range which is desired for IR signature reduction. Opposite thermal behavior has negative dynamic range that is suitable for smart windows and space applications.[21] Although, we have not investigated reduced thermal emission with increased temperature, our tunable absorber structure can also be employed as an intensity tunable thermal emitter and has great potential for reducing IR radiation due to increased temperature.
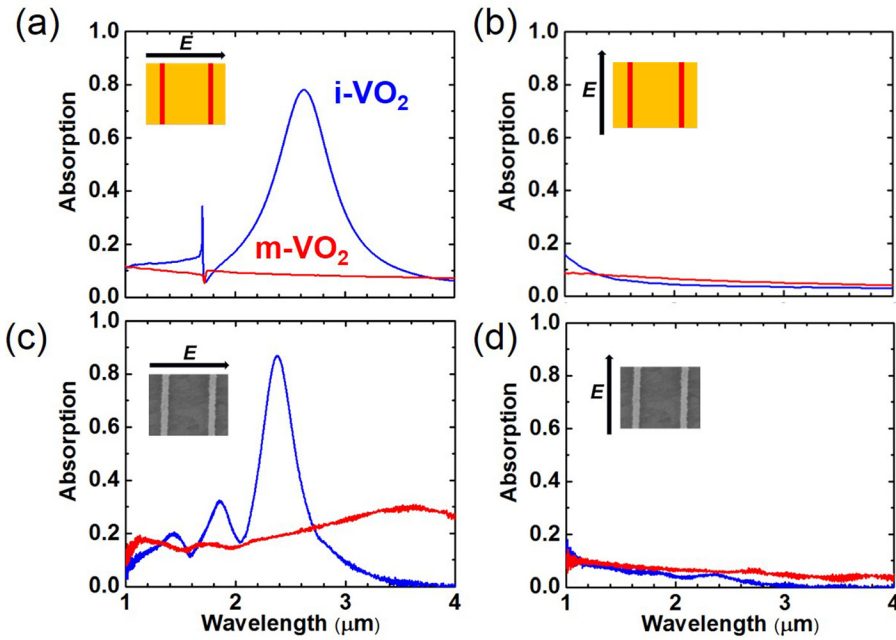
FIG. 2. The absorption characteristics of the grating design tunable IR absorber. (a) and (b) Simulated spectral absorption curves of gold/i-VO$_2$ and gold/m-VO$_2$ composite structures, at perpendicular and parallel polarization relative to grating lines, respectively. Insets: Direction of the electric field vector in relation to the unit cell used in calculations. (c) and (d) Measured spectral absorption curves of gold/i-VO$_2$ and gold/m-VO$_2$ composite structures, at perpendicular and parallel polarization relative to grating lines, respectively. Insets: Direction of the electric field vector in relation to the SEM images of the respective structure. In all graphs, blue curve indicates the i-VO$_2$ (insulator state, room temperature) and the red curve indicates the m-VO$_2$ (metallic state, high temperature).

For certain applications, polarization-independent absorption characteristics are required; therefore, we introduce our second design based on cylindrical gold nanodiscs embedded in VO$_2$ film. Due to symmetry of the square lattice, absorption spectra are independent of the incident electric field polarization. Simulated and measured absorption spectra for c-design are plotted in Figs. 3(a) and 3(b), respectively. Here, the absorption enhancement is approximately 4-fold and 3-fold in simulations and measurements, respectively, for a randomly polarized illumination. Furthermore, simulated (Fig. 3(a)) and measured (Fig. 3(b)) results of our c-design are in fairly good agreement. The similar arguments in g-design IR absorber also apply here to lattice and localized modes. Moreover, structural inhomogeneity of the VO$_2$ film and slight variation in heat conductivity may as well result for minor discrepancies in measured and simulated spectra.

Overall, with both wire and nanodisk Au arrays, we have the ability to control the absorption intensity actively with a high contrast ratio and high positive dynamic range by changing the operation temperature of the device. At low temperatures, VO$_2$ shows insulator characteristics and in both g-design and c-design cases, and metal (Au)–insulator (VO$_2$) nanostructured design creates sharp resonances. At high temperatures, since the VO$_2$ shows metallic characteristics, the material becomes fully reflective and resonant behavior has not been observed. Therefore, the capability of actively controlling the design to switch from one phase to another allows turning the resonance on and off, as a result of the phase transition of VO$_2$.

In order to understand the electric field confinement and absorption mechanism of our absorbers in two phases of VO$_2$ (insulator and metallic), we calculated the power absorption map at the resonance wavelengths of 2.6 μm and 2.3 μm for g-design and c-design, respectively. Absorbed power (P_{abs}) is the divergence of the Poynting vector for non-magnetic materials and can easily be calculated using the simple relation $P_{abs} = \frac{1}{2} \omega \varepsilon_2 |E|^2$, where ω is the angular frequency, ε_2 is the imaginary part of the dielectric permittivity, and $|E|$ is the absolute magnitude of the total electric field.[7,13] The results are shown in Fig. 4 where FDTD simulations were performed with an incident electric field parallel to x-axis. These 3D absorption maps revealed that the absorption mostly takes place in the VO$_2$ layer. It is clear
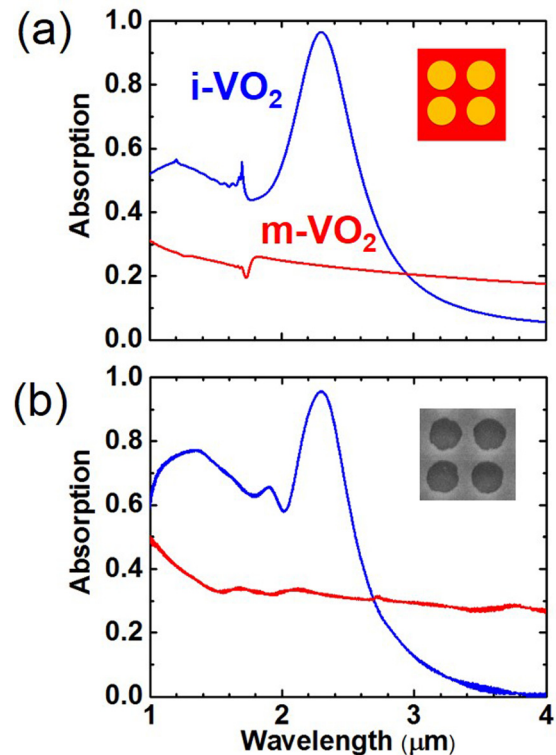

FIG. 3. The absorption characteristics of the cylinder design tunable IR absorber. (a) Simulated spectral absorption curves of gold/i-VO$_2$ and gold/m-VO$_2$ composite structures, Inset: the unit cell used in calculations. (b) Measured spectral absorption curves of gold/i-VO$_2$ and gold/m-VO$_2$ composite structures. Inset: the SEM images of the measured structure. In both graphs, blue curve indicates i-VO$_2$ (insulator state, room temperature) and the red curve indicates m-VO$_2$ (metallic state, high temperature).
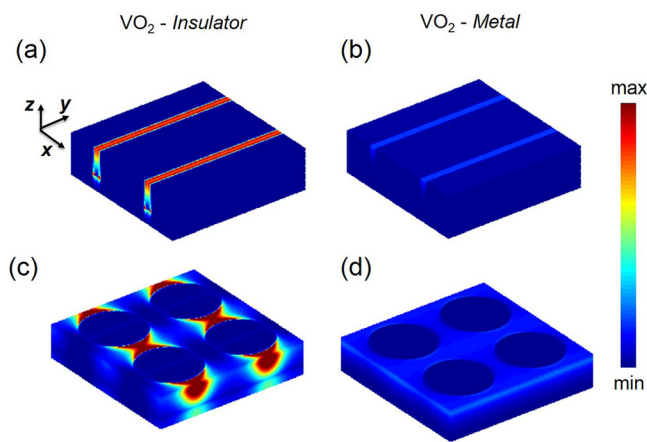
VO$_2$ - *Insulator*   VO$_2$ - *Metal*

FIG. 4. At 2.6 μm resonant wavelength, 3D power absorption (P_{abs}) map of the g-design (a) at room temperature (i-VO$_2$) and (b) at high temperature (m-VO$_2$). At 2.3 μm resonant wavelength, 3D power absorption map of the c-design (c) at room temperature (i-VO$_2$) and (d) at high temperature (m-VO$_2$).

that the i-VO$_2$ (Fig. 4(a)) has stronger absorption compared to the m-VO$_2$ (Fig. 4(b)). Similar behavior is evident for c-design. The absorption is highest in the i-VO$_2$ (Fig. 4(c)) between the gold cylinders along the polarization direction, whereas the m-VO$_2$ layer (Fig. 4(d)) has negligible power absorption compared to the insulating phase. This vast absorption contrast between the two phases of both-design structures is originating from highly localized electric field inside the i-VO$_2$ film. In the insulating phase, in which VO$_2$ behaves like an ordinary lossy dielectric. Therefore, resonance modes of the periodic metallic structure are available for coupling. However, in the metallic phase of VO$_2$, the imaginary part of the dielectric permittivity is so high that field penetration is minimal (see supplementary material.[18]) Therefore, there is no resonance mode available and the incident light is mostly reflected back.

In conclusion, we demonstrated intensity tunable resonant absorber operating at the short-wavelength infrared region by utilizing the phase transition of VO$_2$ via thermal stimulus. By heating up our devices to a temperature roughly of >80 °C, we were able to tune the absorption from 90% to 20% and from 96% to 32% for linearly polarized and unpolarized IR illumination, respectively. This kind of a device finds its use in many practical applications that works in short wave IR spectrum such as short-wave imaging systems.

[1]H. Tao, N. I. Landy, C. M. Bingham, X. Zhang, R. D. Averitt, and W. J. Padilla, Opt. Express **16**(10), 7181–7188 (2008).
[2]Y. Avitzour, Y. A. Urzhumov, and G. Shvets, Phys. Rev. B **79**(4), 045131 (2009).
[3]N. Liu, M. Mesch, T. Weiss, M. Hentschel, and H. Giessen, Nano Lett. **10**(7), 2342–2348 (2010).
[4]T. Cao, L. Zhang, R. E. Simpson, and M. J. Cryan, J. Opt. Soc. Am. B **30**(6), 1580–1585 (2013).
[5]H. Kocer, S. Butun, Z. Li, and K. Aydin, Sci. Rep. **5**, 8157 (2015).
[6]Y. Fei, Z. Hai, J. C. Reed, A. Y. Zhu, and E. Cubukcu, IEEE Photonics Technol. Lett. **26**(2), 202–205 (2013).
[7]K. Aydin, V. E. Ferry, R. M. Briggs, and H. A. Atwater, Nat. Commun. **2**, 517 (2011).
[8]Z. Li, S. Butun, and K. Aydin, ACS Nano **8**(8), 8242–8248 (2014).
[9]S. Butun and K. Aydin, Opt. Express **22**(16), 19457–19468 (2014).
[10]W. Streyer, S. Law, G. Rooney, T. Jacobs, and D. Wasserman, Opt. Express **21**(7), 9113–9122 (2013).
[11]J. J. Talghader, A. S. Gawarikar, and R. P. Shea, Light: Sci. Appl. **1**(8), e24 (2012).
[12]J.-J. Greffet, R. Carminati, K. Joulain, J.-P. Mulet, S. Mainguy, and Y. Chen, Nature **416**(6876), 61–64 (2002).
[13]V. E. Ferry, L. A. Sweatlock, D. Pacifici, and H. A. Atwater, Nano Lett. **8**(12), 4391–4397 (2008).
[14]H. A. Atwater and A. Polman, Nat. Mater. **9**(3), 205–213 (2010).
[15]R. A. Pala, J. White, E. Barnard, J. Liu, and M. L. Brongersma, Adv. Mater. **21**(34), 3504–3509 (2009).
[16]M. J. Dicken, K. Aydin, I. M. Pryce, L. A. Sweatlock, E. M. Boyd, S. Walavalkar, J. Ma, and H. A. Atwater, Opt. Express **17**(20), 18330–18339 (2009).
[17]K. Appavoo and R. F. Haglund, Nano Lett. **11**(3), 1025–1031 (2011).
[18]See supplementary material at http://dx.doi.org/10.1063/1.4918938 for material data used for calculations, E-field distribution discussion, and methods used in growth, fabrication, and calculations.
[19]See http://www.lumerical.com/tcad-products/fdtd/ for Lumerical Solutions, Inc.
[20]C. M. Watts, X. Liu, and W. J. Padilla, Adv. Mater. **24**(23), OP98–OP120 (2012).
[21]R. L. Voti, M. C. Larciprete, G. Leahu, C. Sibilia, and M. Bertolotti, J. Appl. Phys. **112**(3), 034305 (2012).